New insights into the relationship between mass eruption rate and volcanic column height based on the IVESPA dataset

Thomas J. Aubry[1,2]*, Samantha Engwell[3]*, Costanza Bonadonna[4], Larry G. Mastin[5], Guillaume Carazzo[6], Alexa R. Van Eaton[5], David E. Jessop[6,7], Roy G. Grainger[8], Simona Scollo[9], Isabelle A. Taylor[8], A. Mark Jellinek[10], Anja Schmidt[11,12,13], Sébastien Biass[4], Mathieu Gouhier[7]

[1]Department of Earth and Environmental Sciences, University of Exeter, Penryn, UK

[2]Previously at: Sidney Sussex College, University of Cambridge, Cambridge UK

[3]British Geological Survey, The Lyell Centre, Edinburgh

[4]Department of Earth Sciences, University of Geneva, Geneva, Switzerland

[5]U.S. Geological Survey, Cascades Volcano Observatory, Vancouver, Washington, USA

[6]Université de Paris Cité, Institut de physique du globe de Paris, CNRS, F-75005 Paris, France

[7]Université Clermont Auvergne, CNRS, IRD, OPGC Laboratoire Magmas et Volcans, F-63000 Clermont-Ferrand, France

[8]COMET, Atmospheric, Oceanic and Planetary Physics, University of Oxford, Oxford, OX1 3PU, UK

[9]Istituto Nazionale di Geofisica e Vulcanologia, Osservatorio Etneo, Catania, Italy

[10]Earth Ocean and Atmospheric Sciences, University of British Columbia, Vancouver, Canada

[11]Institute of Atmospheric Physics (IPA), German Aerospace Center (DLR), Oberpfaffenhofen, Germany

[12]Meteorological Institute, Ludwig Maximilian University of Munich, Munich, Germany

[13]Department of Chemistry, University of Cambridge, Cambridge, UK

Corresponding author: Thomas J. Aubry (t.aubry@exeter.ac.uk)

*Co-first authors: these authors contributed equally to the publication and either of their names can be used first when citing this work.

Key Points:

- Using 134 volcanic events, we constrain empirical scaling relationships between mass eruption rate and four metrics of column height
- We do not detect a clear influence of atmospheric stratification, wind, and humidity on scaling relationships in this global database
- We discuss limitations of global data and discrepancies between scaling models and the observed behavior of explosive eruptions in nature

Abstract

Relating the mass eruption rate (MER) of explosive eruptions to column height in the atmosphere is key to reconstructing past eruptions and forecasting volcanic hazards. Using 134 eruptive events from the Independent Volcanic Eruption Source Parameter Archive (IVESPA v1.0), we explore the canonical MER-height relationship for four measures of column height: spreading level, sulfur dioxide height, and top height from both directly observed plumes and those reconstructed from deposits. These relationships show significant differences and should be chosen carefully for operational and research applications. The roles of atmospheric stratification, wind, and humidity remain challenging to assess across the large range of eruptive conditions in this database, ultimately resulting in empirical relationships outperforming analytical models that account for atmospheric conditions. This finding reveals the complexity of the height-MER relation that is difficult to constrain based on available heterogeneous observations, which reinforces the need for improved datasets to develop eruptive column models.

Plain Language Summary

Explosive volcanic eruptions expel gas and particles in the form of a volcanic column (or plume) that rises into the atmosphere. Two important metrics characterizing these eruptions are the maximum rise height and the eruptive intensity, i.e. the rate at which material is expelled from the eruptive vent. Understanding the relationship between these parameters is critical for reconstructing past volcanic events and managing hazards during volcanic crises. In this study, we use a new database of well-characterized eruptions to constrain simple relationships between column height and eruptive intensity. We distinguish four different measurements of column height: the maximum height reached by emitted particles from observations and from analysis of deposits, the height at which ash spreads in the atmosphere, and the height reached by volcanic sulfur gases. We show that each height category has a distinct relationship with the eruption intensity, enabling volcanologists and risk managers worldwide to use the relationship most appropriate to the measurements available to them. Despite the improved level of detail, our dataset cannot resolve any systematic influence of atmospheric conditions such as wind and humidity on eruption column height, highlighting that the second-order complexity of individual eruptions cannot be captured by simplified relationships.

1. Introduction

Mass eruption rate (MER) and eruptive column (also known as volcanic plume) height are critical for forecasting volcanic ash transport and dispersion during an eruption (e.g., Mastin et al., 2022). MER and height also help quantify the scale of an eruption (Newhall and Self, 1982; Carey and Sigurdsson, 1989; Crosweller et al., 2012). Although column height can often be directly observed, MER is more challenging to constrain (Pioli and Harris, 2019). Satellite, radar, cameras, or infrasound sensors have been used to directly estimate MER in near real-time (e.g., Bear-Crozier et al., 2020; Freret-Lorgeril et al., 2021; Mereu et al., 2022), but these pioneering applications are either not operational or limited to a few of the world's best-monitored volcanoes (e.g. Etna volcano, Italy). Therefore, computationally inexpensive empirical scaling relationships and one-dimensional (1D) eruptive column models remain the most common tools to estimate MER based on observed height. The scaling models are particularly widely applied owing to their simplicity.

The canonical scaling model is an empirical power law relationship between MER and column height (Morton et al., 1956, Wilson et al., 1978; Sparks et al., 1997, Mastin et al., 2009). Development of these empirical relationships - and the validation of eruptive column models in general (e.g. 1D and 3D) - is limited by datasets with a narrow range of eruptive and atmospheric parameters, absent or sparse information on uncertainty, and the accidental use of dependent data, e.g., when MER is estimated from the column height itself. To address these issues, the Eruption Source Parameters working group of the Commission on Tephra Hazard Modeling of the International Association of Volcanology and Chemistry of the Earth's Interior (IAVCEI) developed the Independent Volcanic Eruption Source Parameter Archive (IVESPA, Aubry et al. 2021). Here, we use IVESPA to explore new empirical relationships between MER and the height of both tephra and SO_2 eruption columns. We also compare these results with analytical scaling models that account for atmospheric conditions.

2. Overview of IVESPA

We use version 1.0 of IVESPA (http://www.ivespa.co.uk/), which is described in Aubry et al. (2021). The database contains 134 eruptive events, i.e. eruption or eruption phases for which we have estimates of tephra fall deposit mass, eruption duration, atmospheric conditions, and column height. Among these events, 111 are small- moderate, 18 are Subplinian and 5 are Plinian (using the Bonadonna and Costa 2013 classification). IVESPA uses the following height metrics (see sketch in Figure 2 in Aubry et al., 2021):

- H_{top} , the height of the top of the tephra column, available for 130 events
- H_{spr} , the spreading height of the tephra cloud, available for 41 events
- H_{SO2} , the height of SO_2 injection, available for 28 events.

The measurement techniques used to estimate heights (e.g., satellite, ground-based radar or lidar, visual observations) are reported although a single best estimate based on all available measurements is provided. Estimates of heights, mass of tephra, and duration are independent, e.g. no tephra mass was estimated by inverting information from column height. We define the MER as the mass of tephra fallout, derived from mapping the tephra fallout deposits and empirical fitting of the thinning trends (e.g., Bonadonna and Costa, 2012), divided by the eruptive event duration. As defined, MER is thus a time-averaged value, and we denote it $\overline{\mathrm{MER}}$. For consistency, IVESPA provides height estimates that are also aimed to be representative of a time-averaged value, denoted by $\overline{\mathrm{H}}_{\mathrm{top}}$, $\overline{\mathrm{H}}_{\mathrm{spr}}$ and $\overline{\mathrm{H}}_{\mathrm{so2}}$.

IVESPA parameters are assigned uncertainties aimed to be representative of a 95% confidence level. Both the best estimates and uncertainties are assigned an interpretation flag value between 0 (no interpretation) and 2 (significant interpretation of the data source(s)). Atmospheric profiles from two climate reanalyses are provided and are time-averaged over each event duration. IVESPA also contains vertically averaged (between the vent and $\overline{\mathrm{H}}_{\mathrm{top}}$) values of the horizontal wind speed ($\overline{\mathrm{W}}$) and stratification (Brunt-Väisälä frequency, $\overline{\mathrm{N}}$). The mean value from both atmospheric reanalyses is used as the best estimate, and their difference (halved) as the uncertainty. Table S1 contains all parameters used in this study and their calculation is detailed in Supporting Information S1 unless directly provided in IVESPA.

Top column heights are commonly estimated from deposits using isopleth contours (e.g. Carey and Sparks, 1986), which are excluded from IVESPA. However, for this study we compile an additional suite of top heights determined from isopleths, which are available for 18 eruptive events in IVESPA. This enables us to test whether $\overline{\mathrm{MER}}$-height relationships derived from directly observed column heights are consistent with isopleth-derived heights. We denote isopleth-derived heights $\mathrm{H}_{\mathrm{iso,top}}$ and do not bar the symbol because they are commonly representative of the maximum rather than time-averaged column height (e.g., Burden et al., 2011). For consistency, we use $\mathrm{H}_{\mathrm{iso,top}}$ estimated using the Carey and Sparks (1986) method rather than more recent and comprehensive methods (Rossi et al., 2019) that account e.g. for wind impact but have been applied to a limited number of events. Supporting Information S2 and Table S2 provide detail on $\mathrm{H}_{\mathrm{iso,top}}$ data collection.

3. Results

3.1 Empirical scaling relationships specific to different column height metrics

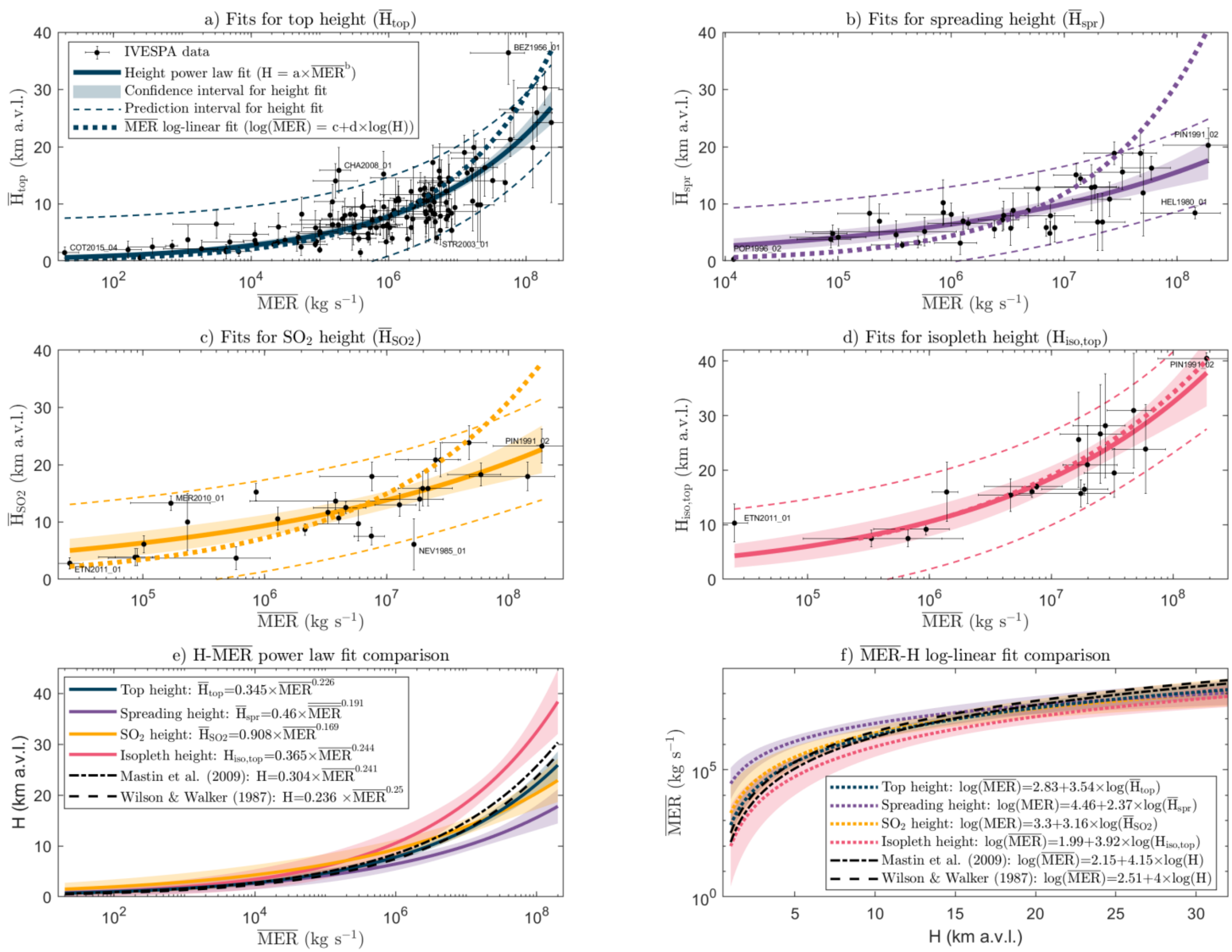

Figure 1. $\overline{H}_{top}$ (a), $\overline{H}_{spr}$ (b), $\overline{H}_{SO2}$ (c) and $H_{iso,top}$ (d) as a function of $\overline{MER}$. Thick continuous lines are the power law fit relationship between heights and $\overline{MER}$, with shading showing the confidence interval, and the thin dashed lines showing the prediction interval. The confidence interval reflects the uncertainty on the fitted model parameters and can be used to test if two models are significantly different. The prediction interval reflects both the uncertainty on the model parameters and the model error and should be used when making a prediction with the model. All uncertainties are at the 95% confidence level. The bold dotted lines show the best linear fit relationship between the logarithm $\overline{MER}$ and the logarithm of heights (logarithm refers to base 10 logarithm in this study). Information on all newly calibrated fits are provided in tabular form in Table S3. Panels e-f show comparison of the fit relationships for the four heights

considered, along with select relationships from previous studies (Wilson and Walker, 1987; Mastin et al., 2009), for the power law (e) and log-linear (f) fits. Select events on panels a-d are labelled using their IVESPA identifiers (see Table S1 for full details): BEZ=Bezymianny, CHA=Chaitén, COT=Cotopaxi, ETN=Etna, HEL=St. Helens, MER=Merapi, NEV=Nevado del Ruiz, PIN=Pinatubo, POP=Popocatépetl, STR=Stromboli.

Figure 1 a–d shows how $\overline{\mathrm{H}}_{\mathrm{top}}$ (a), $\overline{\mathrm{H}}_{\mathrm{spr}}$ (b), $\overline{\mathrm{H}}_{\mathrm{so2}}$ (c) and $\mathrm{H}_{\mathrm{iso,top}}$ (d) relate to $\overline{\mathrm{MER}}$, and corresponding empirical power law relationships using a least-squares fit. $\overline{\mathrm{MER}}$ values in the IVESPA database range from 2×10^1–2×10^8 kg s^{-1} (median: 1.6×10^6 kg s^{-1}), which is a larger range with a higher proportion of low-intensity events compared to previous studies (e.g., Mastin et al. (2009) provide a $\overline{\mathrm{MER}}$ range of 6×10^3–2×10^8 kg s^{-1} with median of 10^7 kg s^{-1}). Defining $\overline{\mathrm{MER}}$ using the total mass of tephra (i.e., including pyroclastic density current contributions instead of fallout only) results in lower coefficients of determination (R^2, Figure S1). For the $\overline{\mathrm{MER}} - \overline{\mathrm{H}}_{\mathrm{top}}$ fit constrained by 130 events, we find best-fit relationships between the $\overline{\mathrm{MER}}$ in kg s^{-1} and $\overline{\mathrm{H}}_{\mathrm{top}}$ in km above vent level (a.v.l.) of:

$$\overline{\mathrm{H}}_{\mathrm{top}} = 0.345 \times \overline{\mathrm{MER}}^{0.226} \quad \text{(Equation 1)}$$

with the $\overline{\mathrm{MER}}$ as independent variable, and

$$\log\left(\overline{\mathrm{MER}}\right) = 2.83 + 3.54 \times \log\left(\overline{\mathrm{H}}_{\mathrm{top}}\right), \text{equivalent to } \overline{\mathrm{H}}_{\mathrm{top}} = 0.159 \times \overline{\mathrm{MER}}^{0.283} \quad \text{(Equation 2)}$$

with $\overline{\mathrm{H}}_{\mathrm{top}}$ as the independent variable and using a log-linear fit. Parameters in Equation 1 are most sensitive to events with high $\overline{\mathrm{MER}}$ values (Figure S2). Best fits for all other types of height are provided in Figure 1 e–f and Table S3, which aims to facilitate use of our new empirical fits, in particular by Volcanic Ash Advisory Centres (VAACs) and Volcano Observatories (VOs). With the exception of $\mathrm{H}_{\mathrm{iso,top}}$, log-linear fits obtained using any of the considered heights as the independent variable predict significantly lower heights for low $\overline{\mathrm{MER}}$ and significantly higher heights for high $\overline{\mathrm{MER}}$ compared to equivalent power law fits calibrated with the $\overline{\mathrm{MER}}$ as the independent variable (Figure 1.a-d).

Figures 1 e–f highlight important differences between empirical fits for different height metrics. For a given $\overline{\mathrm{MER}}$ value, the predicted $\mathrm{H_{iso,top}}$ tends to be significantly higher than the predicted $\overline{\mathrm{H}}_{\mathrm{top}}$ (average $\mathrm{H_{iso,top}}/\overline{\mathrm{H}}_{\mathrm{top}}$ ratio across IVESPA events = 1.45, see Figure S3). This is consistent with the expectation that isopleth-based height reflects an upper bound of the top height, whereas IVESPA top heights aim to reflect a time-averaged value. In addition, the method of Carey and Sparks (1986) tends to overestimate plume height in eruptions in significant wind (Rossi et al., 2019). Unsurprisingly, predicted $\overline{\mathrm{H}}_{\mathrm{spr}}$ tends to be lower than predicted $\overline{\mathrm{H}}_{\mathrm{top}}$, with the average $\overline{\mathrm{H}}_{\mathrm{spr}}/\overline{\mathrm{H}}_{\mathrm{top}}$ ratio of 0.76 in IVESPA matching exactly that predicted by theory for buoyant plumes rising in quiescent stratified environments (Morton et al., 1956; Figure S3). Predicted $\overline{\mathrm{H}}_{\mathrm{top}}$ and $\overline{\mathrm{H}}_{\mathrm{SO2}}$ are generally not significantly different (average $\overline{\mathrm{H}}_{\mathrm{SO2}}/\overline{\mathrm{H}}_{\mathrm{top}}$ ratio is 0.97 in IVESPA, see Figure S3).

The widely used empirical scaling of Mastin et al. (2009) compares best with our $\overline{\mathrm{H}}_{\mathrm{top}}$ fit, although it is closer to our $\mathrm{H_{iso,top}}$ fit at high $\overline{\mathrm{MER}}$s for the power law fit (Fig. 1.e). This finding is not surprising as although the plume height type is unspecified in Mastin et al. (2009), most heights in the literature generally reflect top height values, and Mastin et al. (2009) included isopleth-based column heights in their compilation (unlike IVESPA). Although there are statistically significant differences between the Mastin et al. (2009) and our new top height fits (up to 15% for predicted $\overline{\mathrm{H}}_{\mathrm{top}}$ and up to 0.6 for predicted log($\overline{\mathrm{MER}}$), i.e. a factor of 4 for $\overline{\mathrm{MER}}$), these differences are small relative to the prediction errors of these empirical laws. The relative root mean squared error (RMSE) on $\overline{\mathrm{H}}_{\mathrm{top}}$ (predicted from $\overline{\mathrm{MER}}$) is 53% for Equation 1, 57% for Equation 2 and 60% for Mastin et al. (2009) (Figure S4.a). When using these relationships and observed $\overline{\mathrm{H}}_{\mathrm{top}}$ to invert for $\overline{\mathrm{MER}}$, duration or tephra fallout mass (Fig. S4.b-d), the RMSE on a logarithmic scale is 0.81 for Equation 1, 0.76 for Equation 2 and 0.80 for Mastin et al. (2009). The new empirical relationships for $\overline{\mathrm{H}}_{\mathrm{top}}$ (Equations 1-2) are thus broadly consistent with Mastin et al. (2009). However, we show that the optimal parameter values of empirical scaling relationships and corresponding predictions differ greatly depending on the height metric (i.e. $\overline{\mathrm{H}}_{\mathrm{top}}$, $\overline{\mathrm{H}}_{\mathrm{spr}}$, $\overline{\mathrm{H}}_{\mathrm{SO2}}$ or $\mathrm{H}_{\mathrm{iso,top}}$).

3.2 Accounting for atmospheric conditions using analytical scaling models

Unlike the empirical relationships shown in Figure 1, several analytical (derived from buoyant plume theory) scaling models explicitly account for atmospheric stratification ($\overline{N}$) and horizontal wind speed $\overline{(W)}$. Here use IVESPA to evaluate five of these models (Morton et al., 1956, Hewett et al., 1971, Degruyter and Bonadonna, 2012, Woodhouse et al., 2013 and Aubry et al., 2017; see details in Table 1 and Supporting Text S3). Table 1 ("unweighted" column) provides the adjusted R^2 when using the $\overline{\mathrm{MER}}$ and atmospheric conditions as independent variables, and $\overline{\mathrm{H}}_{\mathrm{top}}$ as the dependent variable. The only model that outperforms the empirical relationship between $\overline{\mathrm{H}}_{\mathrm{top}}$ and $\overline{\mathrm{MER}}$ (Equation 1, $R^2 = 0.67$) is another empirical power law between $\overline{\mathrm{H}}_{\mathrm{top}}$, $\overline{\mathrm{MER}}$, $\overline{N}$ and $\overline{W}$ ($R^2 = 0.75$). However, the obtained exponent for $\overline{N}$ is 1.1, meaning that higher column heights are obtained for stronger stratification values, which is an unphysical result (Morton et al., 1956). The analytical scaling models have R^2 values between 0.32 and 0.52, much smaller than the empirical power law. This finding cannot be explained by the fact that we use the same dataset to calibrate Equation 1 and calculate corresponding R^2 because the Mastin et al. (2009) relationship also has a higher R^2 (0.62) than analytical scalings despite being calibrated against a much smaller dataset (Aubry et al., 2021).

The poor performance of analytical scaling relationships could be explained by poorly constrained parameter values in IVESPA, or the fact that specific eruptions dominate the database. To explore these possibilities, in Table 1, we give different weight to events in the database according to their characteristics (Supporting Information S4):

- In column 4 (“Eruption”), we give the same weight to each eruption in IVESPA (e.g., the 18 events from the 1989-1990 Mt Redoubt eruption have the same weight as the two events from the 1991 Mt. Pinatubo eruption).

- In column 5 (“Uncertainty”), weights are inversely proportional to the uncertainty on the observed and predicted $\overline{\mathrm{H}}_{\mathrm{top}}$ values for each event, the former being linked to $\overline{\mathrm{MER}}$ uncertainty.

- In column 6 (“Interpretation flag”), less weight is given to events that required significant interpretation of the literature to attribute $\overline{\mathrm{H}}_{\mathrm{top}}$ and $\overline{\mathrm{MER}}$ values.

- In column 7 (“All”), the events are weighted according to the product of weights in columns 4-6 to account for all three factors above.

We find that these weighting procedures do not change the main results: i) the empirical power law fit between $\overline{\mathrm{H}}_{\mathrm{top}}$ and $\overline{\mathrm{MER}}$ still outperforms the analytical scaling models in terms of R^2; and ii) the best-performing model is still the empirical power law that includes $\overline{N}$ and $\overline{W}$ terms, and gives a positive (unphysical) exponent for $\overline{N}$. When weighting the eruptive events by parameter uncertainty, the performance of all scaling models improves, with greater improvement among the analytical models accounting for atmospheric conditions. For example, the difference in R^2 values between the power-law fit and the best analytical scaling (Degruyter et al., 2012) when applying all weighting procedures is 0.06, whereas it is 0.19 unweighted. For the power law fit, the $\overline{\mathrm{MER}}$ exponent varies between 0.21 and 0.25 depending on the weighting procedures applied and is thus relatively robust. However, for more complex models, fit parameters are very sensitive to the weighting. For example, the calibrated value of entrainment coefficient ratio β/α in the Aubry et al. (2017) scaling model ranges between -0.43 (an unphysical value) and 4.4. Laboratory studies suggest that the ratio of β/α should be 0.6- 20 (see Aubry and Jellinek, 2018, and references therein). We note that the Hewett et al. (1971) scaling model consistently has the smallest R^2 values, and we always find unphysical parameter values for the Woodhouse et al.

(2013) scaling model, possibly due to their use of a simplified linear wind profile (see Figure S5).

Reference	**Expression for $\overline{\mathbf{H}}_{\mathbf{top}}$**	**Weighting procedure**				
		Unweighted	**Eruption**	**Uncertainty**	**Interpretation flag**	**All**
Empirical power law with coefficients from Mastin et al. (2009)	$0.304\ \overline{\mathrm{MER}}^{0.241}$	R^2=0.62	R^2=0.67	R^2=0.68	R^2=0.65	R^2=0.79
Empirical power law with coefficients calibrated herein	$a\ \overline{\mathrm{MER}}^{b}$	**R^2=0.67, a=0.34, b=0.23**	**R^2=0.7, a=0.46, b=0.21**	**R^2=0.74, a=0.23, b=0.25**	**R^2=0.69, a=0.32, b=0.23**	**R^2=0.81, a=0.25, b=0.25**
Empirical power law accounting for wind and	$a\ \overline{\mathrm{MER}}^{b}\overline{N}^{c}\overline{W}^{d}$	R^2=0.75, a=89, b=0.17, c=1.1, d=-0.049	R^2=0.79, a=1.2e+02, b=0.16, c=1.1, d=-0.0048	R^2=0.75, a=2.4, b=0.24, c=0.48, d=-0.013	R^2=0.74, a=49, b=0.18, c=0.94, d=-0.07	R^2=0.81, a=2.1, b=0.23, c=0.46, d=0.016

stratification						
Morton et al. (1956)*	a $\overline{\mathrm{MER}}^{0.25}\overline{N}^{-0.75}$	R^2=0.49, a=0.0091	R^2=0.51, a=0.0095	R^2=0.68, a=0.0087	R^2=0.53, a=0.0094	R^2=0.75, a=0.0096
Hewett et al. (1971)*	a $\overline{\mathrm{MER}}^{0.33}\overline{N}^{-0.66}\overline{W}^{-0.33}$	R^2=0.32, a=0.0072	R^2=0.29, a=0.0069	R^2=0.58, a=0.0084	R^2=0.42, a=0.0077	R^2=0.63, a=0.0088
Degruyter et al. (2012)*	a $\overline{\mathrm{MER}}^{0.25}\overline{N}^{-0.75}f_{D12}(V^*,b)$	R^2=0.48, a=0.0092, b=0.052	R^2=0.5, a=0.0089, b=-0.2	R^2=0.68, a=0.0091, b=0.11	R^2=0.54, a=0.01, b=0.27	R^2=0.75, a=0.01, b=0.13
Woodhouse et. al (2013)*	a $\overline{\mathrm{MER}}^{0.25}\overline{N}^{-0.75}f_{W13}(W_s,\beta/\alpha)$	R^2=0.52, a=0.011, β/α=-6.8	R^2=0.53, a=0.011, β/α=-5.7	R^2=0.69, a=0.01, β/α=-5.5	R^2=0.58, a=0.011, β/α=-7.1	R^2=0.75, a=0.011, β/α=-3.7
Aubry et al. (2017)*	a $\overline{\mathrm{MER}}^{0.25}\overline{N}^{-0.75}f_{A17}(W^*,\beta/\alpha)$	R^2=0.51, a=0.0099, β/α=2.5	R^2=0.51, a=0.0093, β/α=-0.43	R^2=0.69, a=0.0099, β/α=3.5	R^2=0.58, a=0.011, β/α=4.4	R^2=0.74, a=0.0098, β/α=0.48

Table 1. Adjusted R^2 and calibrated parameter values for tested scaling models, for various weights applied to each IVESPA event (see sections 3.2 and S4). * indicate analytical models. Physical parameters V^*, W_s, W^* and β/α and functional expressions f_{D12}, f_{W13} and f_{A17} are provided in Supporting Information S3. Orange shading highlights models with calibrated

parameter values deemed non-physical. For all other models, bold text highlights the one that has the highest R^2 value.

4. Discussion

4.1 Influence of atmospheric conditions

Using 25 eruptive events, Mastin (2014) demonstrated that a 1D plume model accounting for atmospheric conditions was not as good as an empirical power-law in predicting $\overline{\mathrm{MER}}$ from column height. Despite having improved data compilation methodologies and over 5 times more events in IVESPA (Aubry et al., 2021), we reach similar conclusions as the simple $\overline{\mathrm{MER}}$-$\overline{\mathrm{H}}_{\mathrm{top}}$ empirical power law outperforms analytical scaling models accounting for atmospheric conditions (Table 1). To understand this result, we define the standardized $\overline{\mathrm{H}}_{\mathrm{top}}$ as the ratio of the observed $\overline{\mathrm{H}}_{\mathrm{top}}$ to that predicted by Equation 1 (i.e. $\overline{\mathrm{H}}_{\mathrm{top}}/[0.0345\overline{\mathrm{MER}}^{0.226}]$). This variable expresses how high $\overline{\mathrm{H}}_{\mathrm{top}}$ is relative to the value expected from the $\overline{\mathrm{MER}}$ alone. Figure 2a suggests that the standardized $\overline{\mathrm{H}}_{\mathrm{top}}$ does not depend on the Brunt Väisälä frequency $\overline{\mathrm{N}}$ in IVESPA, whereas some of the results in Table 1 even suggest that $\overline{\mathrm{H}}_{\mathrm{top}}$ increases with $\overline{\mathrm{N}}$ (empirical power-law with $\overline{\mathrm{N}}$ and $\overline{\mathrm{W}}$ terms). These results contradict theoretical and experimental evidence that $\overline{\mathrm{H}}_{\mathrm{top}}$ should decrease in a more strongly stratified atmosphere (e.g. Morton et al., 1956; Woods, 1988), and explain the poor performance of analytical scaling models in which $\overline{\mathrm{H}}_{\mathrm{top}}$ is proportional to $\overline{\mathrm{N}}^{-0.75}$ (Table 1). One potential explanation is that $\overline{\mathrm{N}}$ generally increases with altitude (Figure S5a) and in turn with $\overline{\mathrm{H}}_{\mathrm{top}}$ and $\overline{\mathrm{MER}}$. If $\overline{\mathrm{N}}$ is normalised for each event by the value obtained from the average atmospheric profile across IVESPA (which removes the dependence of $\overline{\mathrm{N}}$ on vent and column altitude), it becomes negatively although insignificantly correlated with the standardized $\overline{\mathrm{H}}_{\mathrm{top}}$ (Figure S6.a).

Figure 2b shows that the standardized top height decreases with stronger horizontal wind speed $\overline{\mathrm{W}}$, as expected from laboratory experiments (e.g., Hewett et al., 1971; Carazzo et al., 2014) and a few well-observed eruptions (e.g., Poulidis et al., 2019). The two variables are not significantly correlated despite the large range of $\overline{\mathrm{W}}$ values in IVESPA (3–41 m s^{-1}). We also do not detect any influence of relative humidity (Figure 3c), despite model predictions that the atmospheric water vapour entrained into a volcanic plume and the associated latent heat and buoyancy flux should boost $\overline{\mathrm{H}}_{\mathrm{top}}$ by over 5 km for small-moderate eruptions in a wet tropical atmosphere (e.g., Woods, 1993; Glaze et al., 1997; Herzog et al., 1998; Tupper et al., 2009). Although several studies have noted that tropical volcanic plumes commonly reach the tropopause (e.g., Tupper and Wunderman, 2009; Carboni et al., 2016), without any constraint on MER as in this study, the role of humidity can only be speculated. Removing the influence of altitude on $\overline{\mathrm{W}}$ and relative humidity (Figure S5) only marginally increases their apparent influence on the standardized top height (Figure S6).

Last, we tested the influence of volcanic plume morphology (i.e., weak, bent-over and spreading downwind only, versus strong, spreading both upwind and downwind). This parameter is explicitly constrained for 44 events in IVESPA, so we complement it by calculating

$$\Pi = \left(\frac{\alpha}{\beta}\right)^2 \frac{\overline{\mathrm{H}}_{\mathrm{top}}\,\overline{N}}{1.8\,\overline{W}} \quad \text{(Equation 3)}$$

for each event. Π is a non-dimensional parameter defined by the ratio of the wind entrainment and plume rise timescales (Degruyter and Bonadonna, 2012) and has been shown to relate to the plume morphology for a handful of eruptions (e.g., Bonadonna et al., 2015b). We use α=0.1 and β=0.55 (Aubry and Jellinek, 2018) in Equation 3. Π values in IVESPA range from 0.02 to 1.1 with weak plumes associated with lower values. Both types of plumes are found for $0.03 < \Pi < 0.35$ (Figures 2d and S3), suggesting a transition from weak to strong plumes at a critical value of $\Pi \approx 0.1$, in agreement with the values used operationally at Mount Etna (Scollo et al., 2019). Despite the absence of any clear relationship between the standardized $\overline{\mathrm{H}}_{\mathrm{top}}$ and Π in Fig. 2d, the variables are significantly correlated, which hints to a small but discernible influence of the plume morphology on the $\overline{\mathrm{H}}_{\mathrm{top}}$ - $\overline{\mathrm{MER}}$ relationship.

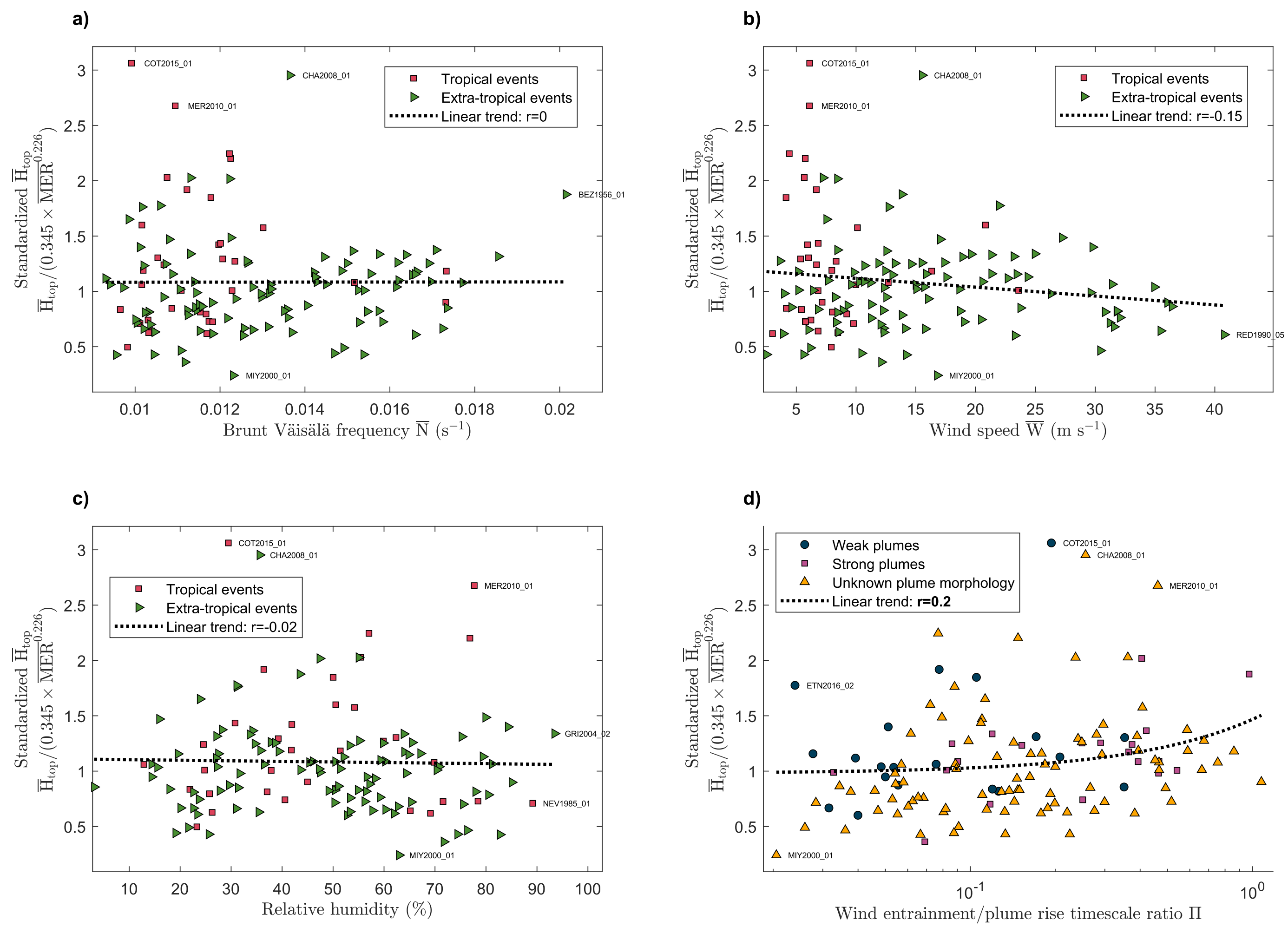

Figure 2. Standardized $\overline{\mathrm{H}}_{\mathrm{top}}$ (i.e. ratio of observed $\overline{\mathrm{H}}_{\mathrm{top}}$ and that predicted by Equation 1 based on $\overline{\mathrm{MER}}$ value) plotted as a function of $\overline{N}$ (a), $\overline{W}$ (b), average relative humidity (c), and Π (d). Linear trends are highlighted by the dotted dashed lines with correlation coefficient r annotated

on each panel (bold if significant at the 95% confidence level). GRI= Grímsvötn, MIY=Miyakejima, RED=Redoubt; see Figure 1 for other acronyms.

4.2 Influence of location and column height measurement technique

Figure 3a shows the distribution of standardized $\overline{\mathrm{H}}_{\mathrm{top}}$ for 10 geographical regions. Across these regions, the median standardized $\overline{\mathrm{H}}_{\mathrm{top}}$ varies between 0.72 and 1.24, i.e. the median $\overline{\mathrm{H}}_{\mathrm{top}}$ differs from the median value predicted using Equation 1 by -28% (Redoubt) to +24% (Central America). The distributions of standardized $\overline{\mathrm{H}}_{\mathrm{top}}$ for these two regions significantly differ compared to all other regions. Differences across the 10 considered regions might reflect a range of factors including atmospheric conditions or the prevalence of certain magma or edifice types. Non-physical factors might also be at play, e.g. the prevalence of island volcanoes which would affect tephra fallout mass and $\overline{\mathrm{MER}}$ estimates due to limited deposition on land. Even when subdivided into 10 geographical areas, most still contain 10-24 events. We can thus calibrate region or volcano-specific $\overline{\mathrm{H}}_{\mathrm{top}}$ - $\overline{\mathrm{MER}}$ relationships and show select examples in Figure 3.c.

Figure 3.b shows the distribution of standardized $\overline{\mathrm{H}}_{\mathrm{top}}$ for 8 different combinations of measurement technique used to measure $\overline{\mathrm{H}}_{\mathrm{top}}$. Standardized $\overline{\mathrm{H}}_{\mathrm{top}}$ issued from satellite-only measurements or a combination of satellite and ground-based instrumental measurements (e.g., radar) are higher than for other measurement techniques (p-value<0.1), consistent with Tupper and Wunderman (2009). In contrast, when visual measurements (ground or aircraft) were used alone or in combination with satellite imagery, the standardized $\overline{\mathrm{H}}_{\mathrm{top}}$ tends to be lower (p-value<0.15). Figure 3d shows that the unique $\overline{\mathrm{H}}_{\mathrm{top}}$ -$\overline{\mathrm{MER}}$ relationships for these two categories (satellite versus ground based measurements) differ significantly at most $\overline{\mathrm{MER}}$ values, although the predicted $\overline{\mathrm{H}}_{\mathrm{top}}$ differ at most by 2 km for $\overline{\mathrm{MER}}<10^8$ kg/s. The dependence of standardized $\overline{\mathrm{H}}_{\mathrm{top}}$ on other parameters was explored with examples for duration and median grain size shown in Figure S7. The 17 events with a duration smaller than 10 times the plume rise timescale tend to have smaller standardized $\overline{\mathrm{H}}_{\mathrm{top}}$ (Figure S7.a) but giving these short-duration events less weights does not change Table 1 results.

Last, for each sub-category shown in Figure 3a and 3b, we annotate the correlation coefficient between the logarithm of the standardized $\overline{\mathrm{H}}_{\mathrm{top}}$ and that of the wind speed $\overline{\mathrm{W}}$. This correlation is only significant for the subgroup of satellite and ground-based $\overline{\mathrm{H}}_{\mathrm{top}}$ measurement (r = -0.87). Negative correlations are expected, but we find a positive correlation for some event groups, e.g., for Icelandic eruptions (r = 0.34, Figure 3.a). This finding further emphasises the difficulty of detecting atmospheric influence on the $\overline{\mathrm{H}}_{\mathrm{top}}$-$\overline{\mathrm{MER}}$ relationship in IVESPA v1.0.

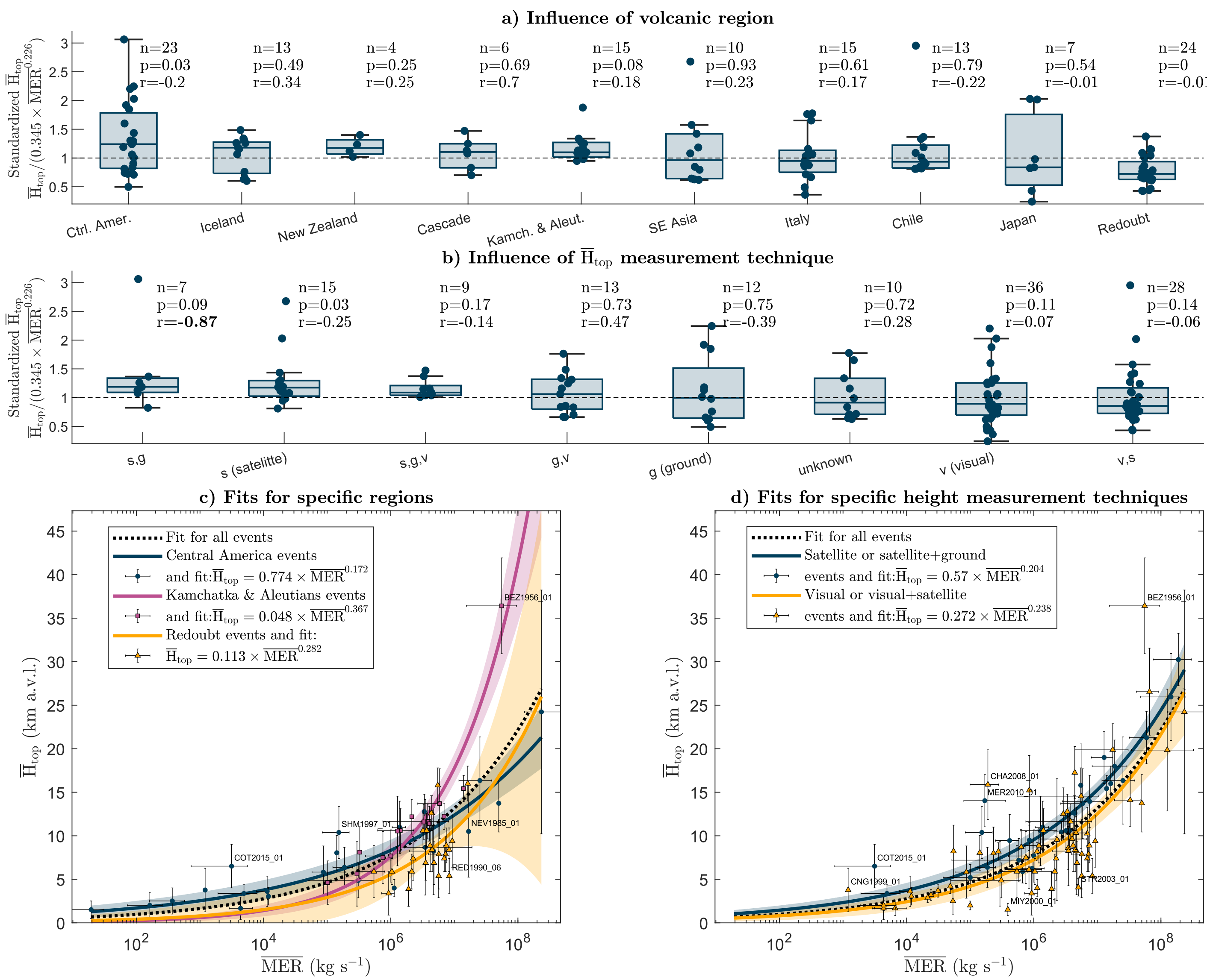

Figure 3. Distribution of the standardized $\overline{\mathrm{H}}_{\mathrm{top}}$ for specific volcanic regions (a) or $\overline{\mathrm{H}}_{\mathrm{top}}$ measurement techniques (b). Box plots show the minimum, quartiles, and maximum values.

Three values are annotated for each subgroup: the number of events (n), the p-value resulting from a Mann-Whitney U-test testing the probability that values from the subgroup differ significantly from the values from all other subgroups (p), and the correlation coefficient between the logarithm of the standardized $\overline{\mathrm{H}}_{\mathrm{top}}$ and the logarithm of $\overline{\mathrm{W}}$ (r, in bold if significant at the 95% level). Panels c-d are similar to Figure 1.a, but show $\overline{\mathrm{H}}_{\mathrm{top}}$ -$\overline{\mathrm{MER}}$ power law fits calibrated for select subgroups of regions (c) or measurement techniques (d). CNG= Cerro Negro, SHM= Soufrière Hills Montserrat; see Figures 1-2 for other labels.

4.3 Measuring eruptions for estimating MER-H relationships

The challenging detection of atmospheric influences on the MER-column height relationship in IVESPA v1.0 may be due to the use of 0D scaling models, and future studies could investigate application of more sophisticated eruptive column models (e.g.. 1D, 3D) or data analysis techniques (e.g. machine learning) to IVESPA. However, our study hints at developments of IVESPA, and eruptive data more generally, that will help build a better understanding of the relationship between MER and column height. First, Figure 3.b shows that future versions of IVESPA should separate column heights according to measurement type instead of providing one height value and a list of measurements type used to derive it. Second, Figure 3.a and other studies suggest that compiling information such as magma composition or type (e.g. Trancoso et al., 2022) and conduit information (e.g. Gouhier et al., 2019) would help constrain other factors modulating the relationship between height and MER. In terms of atmospheric conditions, one open question is how well large-scale reanalysis datasets resolve meterological variability at the scale of volcanic edifices. Last, a challenging question is whether the use of time-averaged eruption source parameters enable detection of atmospheric influence on plume dynamics in a database with such a variety of eruptions. Advances in near real-time measurements of MER (Caudron et al., 2015; Freret-Lorgeril et al., 2018, 2021; Bear-Crozier et al., 2020; Mereu et al. 2022) might unlock the potential to provide time series of parameters for both height and MER for many events. Such collection of time series would provide a step change in assessing MER – column height relationships.

5 Conclusions

We used the new Independent Volcanic Eruption Source Parameter Archive (IVESPA, Aubry et al., 2021) to explore the empirical power law relationship linking eruptive column height to MER. A key improvement over previous work is that our new relationships are specific to the type of column height considered, i.e. the height of the SO_2 cloud ($\overline{\mathrm{H}}_{\mathrm{SO2}}$), the spreading height of the tephra cloud ($\overline{\mathrm{H}}_{\mathrm{spr}}$), and the top height of the ash cloud directly measured ($\overline{\mathrm{H}}_{\mathrm{top}}$) or derived from the deposit ($\mathrm{H}_{\mathrm{iso,top}}$) with significant differences among these four metrics (Figure 1 and S3). We recommend that users such as VAACs or VOs apply the relationship most adapted to their available height measurement type, and we provide extensive details on each calibrated relationship and their uncertainties in Table S3. The newly calibrated power law relationship between $\overline{\mathrm{H}}_{\mathrm{top}}$ and $\overline{\mathrm{MER}}$ (Equation 1) still results in discrepancies of 50% for predicted $\overline{\mathrm{H}}_{\mathrm{top}}$, and a factor of ~6 for predicted $\overline{\mathrm{MER}}$ (Figures 1 and S4). Despite such large discrepancies, this empirical power law outperforms analytical scaling models accounting for atmospheric conditions (Table 1). This is an interesting result given the extensive body of literature describing the influence of wind, humidity, and atmospheric stratification on eruption column behaviour. Our inability to detect a statistically significant influence of these atmospheric properties on column heights in the improved database suggests several possibilities. First, further improvements to IVESPA might be needed such as better consistency and distinctions in methods used to estimate $\overline{\mathrm{H}}_{\mathrm{top}}$ (e.g. satellite, radar, visual) and $\overline{\mathrm{MER}}$ (e.g. empirical model used to fit thinning trends). Second, analysis of the $\overline{\mathrm{H}}_{\mathrm{top}}$-$\overline{\mathrm{MER}}$ relationship using more sophisticated models than scaling relationships, such as 1D and 3D plume models, may be required. And third, we may simply be identifying an inherent limitation in the accuracy with which we capture time-averaged plume heights or erupted mass by deposit mapping. In other words, defining a relationship based on widely varying magmatic conditions, eruption styles, atmospheric conditions, and measurement techniques helps reveal first-order controls on column height, but obscures the nuances of eruption behaviour that are apparent on a case-by-case basis.

Acknowledgments

We sincerely thank Frances Beckett and Marcus Bursik for discussions that significantly improved the manuscript. TJA was supported by the Sidney Sussex College through a Junior Research Fellowship. SLE was supported by the Global Geological Risk Research Platform of the British Geological Survey NC-ODA grant NE/R000069/1: Geoscience for Sustainable Futures and the European Union's Horizon 2020 project EUROVOLC (grant agreement no. 731070) and publishes with permission of the CEO, British Geological Survey. This is LabEx ClerVolc contribution number 570. IAT and RGG's effort was partly supported by NERC grants VPLUS (NE/S004025/1) and R4-Ash (NE/S003843/1) as well as the NERC Centre for the Observation and Modelling of Earthquakes, Volcanoes and Tectonics (COMET), a partnership between UK Universities and the British Geological Survey. We thank the British Geological Survey for supporting the IVESPA project and hosting the database website (ivespa.co.uk). Any use of trade, firm, or product names is for descriptive purposes only and does not imply endorsement by the U.S. Government.

Open Research

All data used in this study is available from the Independent Volcanic Eruption Source Parameter Archive (IVESPA) Version 1.0 at http://ivespa.co.uk/data.html . IVESPA is curated by the IAVCEI Commission on Tephra Hazard Modelling and supported by the British Geological Survey.

References

Andronico, D., Scollo, S., Cristaldi, A., & Castro, M. D. L. (2014). Representivity of incompletely sampled fall deposits in estimating eruption source parameters: a test using the 12–13 January 2011 lava fountain deposit from Mt. Etna volcano, Italy. Bulletin of volcanology, 76(10), 861. https://doi.org/10.1007/s00445-014-0861-3

Aubry, T. J., Jellinek, A. M., Carazzo, G., Gallo, R., Hatcher, K., & Dunning, J. (2017). A new analytical scaling for turbulent wind-bent plumes: Comparison of scaling laws with analog experiments and a new database of eruptive conditions for predicting the height of volcanic plumes. Journal of Volcanology and Geothermal Research, 343, 233-251.

Aubry, T. J., Engwell, S., Bonadonna, C., Carazzo, G., Scollo, S., Van Eaton, A.R., Taylor, I.A., Jessop, D., Eychenne, J., Gouhier, M., Mastin, L.G., Wallace, K.L., Biass, S., Bursik, M., Grainger, R.G., Jellinek, A.M., Schmidt, A. (2021). The Independent Volcanic Eruption Source Parameter Archive (IVESPA, version 1.0): A new observational database to support explosive eruptive column model validation and development. Journal of Volcanology and Geothermal Research, https://doi.org/10.1016/j.jvolgeores.2021.107295

Aubry, T. J. and A. M. Jellinek (2018), New insights on entrainment and condensation in volcanic plumes: Constraints from independent observations of explosive eruptions and implications for assessing their impacts, Earth and Planetary Science Letters, 490, 132-142, https://doi.org/10.1016/j.epsl.2018.03.028

Bear-Crozier, A., Pouget, S., Bursik, M. et al. (2020) Automated detection and measurement of volcanic cloud growth: towards a robust estimate of mass flux, mass loading and eruption duration. Nat Hazards 101, 1–38 . https://doi.org/10.1007/s11069-019-03847-2

Bonadonna, C., Costa, A., 2012. Estimating the volume of tephra deposits: a new simple strategy. Geology G32769–1. http://dx.doi.org/10.1130/G32769.1.

Bonadonna, C., Costa, A. Plume height, volume, and classification of explosive volcanic eruptions based on the Weibull function. Bull Volcanol 75, 742 (2013). https://doi.org/10.1007/s00445-013-0742-1

Bonadonna, C., Cioni, R., Pistolesi, M., Elissondo, M., Baumann, V., (2015a). Sedimentation of long-lasting wind-affected volcanic plumes: the example of the 2011 rhyolitic Cordón Caulle eruption, Chile. Bull. Volcanol. 77 (2), 13. http://dx.doi.org/10.1007/s00445-015-0900-8.

Bonadonna, C., Pistolesi, M., Cioni, R., Degruyter, W., Elissondo, M., & Baumann, V. (2015b). Dynamics of wind-affected volcanic plumes: The example of the 2011 Cordón Caulle eruption, Chile. Journal of Geophysical Research: Solid Earth, 120(4), 2242-2261.

Bonadonna, C., S. Biass, A. Costa (2015c), Physical characterization of explosive volcanic eruptions based on tephra deposits: propagation of uncertainties and sensitivity analysis J. Volcanol. Geotherm. Res., 296 (2015), pp. 80-100, 10.1016/j.jvolgeores.2015.03.009

Bourdier, J.-L., Pratomo, I., Thouret, J.-C., Boudon, G., Vincent, P.M., (1997) Observations, stratigraphy and eruptive processes of the 1990 eruption of Kelut volcano, Indonesia. J. Volcanol. Geotherm. Res. 79 (3), 181–203. http://dx.doi.org/10.1016/S0377-0273(97)00031-0.

Burden R.E., Phillips J.C., Hincks T.K. (2011) Estimating volcanic plume heights from depositional clast size. Journal of Geophysical Research-Solid Earth 116: B11206 doi:10.1029/2011JB008548

Carazzo, G., Girault, F., Aubry, T., Bouquerel, H., & Kaminski, E. (2014). Laboratory experiments of forced plumes in a density-stratified crossflow and implications for volcanic plumes. Geophysical Research Letters, 41(24), 8759-8766.

Carboni, E., Grainger, R., Mather, T. A., Pyle, D. M., Dudhia, A., Thomas, G., ... & Balis, D. (2016). The vertical distribution of volcanic SO2 plumes measured by IASI. Atmospheric Chemistry and Physics, 16. doi:10.5194/acpd-15-24643-2015

Carey, S., Sparks, R.S.J. (1986) Quantitative models of the fallout and dispersal of tephra from volcanic eruption columns. Bull Volcanol 48, 109–125 . https://doi.org/10.1007/BF01046546

Carey, S., Sigurdsson, H. (1986) The 1982 eruptions of El Chichon volcano, Mexico (2): Observations and numerical modelling of tephra-fall distribution. Bull Volcanol 48, 127–141 . https://doi.org/10.1007/BF01046547

Carey, S., Sigurdsson, H. (1989) The intensity of plinian eruptions. Bull Volcanol 51, 28–40 . https://doi.org/10.1007/BF01086759

Carey, S., Sigurdsson, H., Gardner, J. E., & Criswell, W. (1990). Variations in column height and magma discharge during the May 18, 1980 eruption of Mount St. Helens. Journal of Volcanology and Geothermal Research, 43(1-4), 99-112. https://doi.org/10.1016/0377-0273(90)90047-J

Castruccio, A., Clavero, J., Segura, A. et al. (2016) Eruptive parameters and dynamics of the April 2015 sub-Plinian eruptions of Calbuco volcano (southern Chile). Bull Volcanol 78, 62 . https://doi.org/10.1007/s00445-016-1058-8

Caudron, C., Taisne, B., Garcés, M., Alexis, L. P., & Mialle, P. (2015). On the use of remote infrasound and seismic stations to constrain the eruptive sequence and intensity for the 2014 Kelud eruption. Geophysical Research Letters, 42(16), 6614-6621.

Crosweller, H.S., Arora, B., Brown, S.K., Cottrell, E., Deligne, N.I., Guerrero, N.O., Hobbs, L., Kiyosugi, K., Loughlin, S.C., Lowndes, J. and Nayembil, M., (2012) Global database on large magnitude explosive volcanic eruptions (LaMEVE). Journal of Applied Volcanology, 1(1), p.4.

Degruyter, W., and Bonadonna, C. (2012), Improving on mass flow rate estimates of volcanic eruptions, Geophys. Res. Lett., 39, L16308, doi:10.1029/2012GL052566.

Eychenne, J., Le Pennec, JL., Troncoso, L. et al. (2012) Causes and consequences of bimodal grain-size distribution of tephra fall deposited during the August 2006 Tungurahua eruption (Ecuador). Bull Volcanol 74, 187–205 . https://doi.org/10.1007/s00445-011-0517-5

Freret-Lorgeril, V., Donnadieu, F., Scollo, S., Provost, A., Fréville, P., Guéhenneux, Y., ... & Coltelli, M. (2018) Mass Eruption Rates of Tephra Plumes During the 2011–2015 Lava Fountain Paroxysms at Mt. Etna From Doppler Radar Retrievals, Frontiers in Earth Sciences, 6, 73.

Freret-Lorgeril, V.; Bonadonna, C.; Corradini, S.; Donnadieu, F.; Guerrieri, L.; Lacanna, G.; Marzano, F.S.; Mereu, L.; Merucci, L.; Ripepe, M.; Scollo, S.; Stelitano, D. (2021) Examples of Multi-Sensor Determination of Eruptive Source Parameters of Explosive Events at Mount Etna. Remote Sens. , 13, 2097. https://doi.org/10.3390/rs13112097

Glaze, L. S., Baloga, S. M., and Wilson, L. (1997), Transport of atmospheric water vapor by volcanic eruption columns, J. Geophys. Res., 102(D5), 6099– 6108, doi:10.1029/96JD03125.

Girault, F., Carazzo, G., Tait, S., Ferrucci, F., & Kaminski, É. (2014). The effect of total grain-size distribution on the dynamics of turbulent volcanic plumes. Earth and Planetary Science Letters, 394, 124-134, https://doi.org/10.1016/j.epsl.2014.03.021

Gouhier, M., Eychenne, J., Azzaoui, N., Guillin, A., Deslandes, M., Poret, M., Costa, A. and Husson, P., 2019. Low efficiency of large volcanic eruptions in transporting very fine ash into the atmosphere. Scientific reports, 9(1), pp.1-12.

Herzog, M., H.-F. Graf, C. Textor, and J. M. Oberhuber (1998), The effect of phase changes of water on the development of volcanic plumes, J. Volcanol. Geotherm. Res., 87, 55– 74, doi:10.1016/S0377-0273(98)00100-0.

Hewett, T. A., Fay, J. A., & Hoult, D. P. (1971). Laboratory experiments of smokestack plumes in a stable atmosphere. Atmospheric Environment (1967), 5(9), 767-789.

Kratzmann, D.J., Carey, S.N., Fero, J., Scasso, R.A., Naranjo, J.-A., (2010) Simulations of tephra dispersal from the 1991 explosive eruptions of Hudson volcano, Chile. J. Volcanol. Geotherm. Res. 190 (3), 337–352. http://dx.doi.org/10.1016/j.jvolgeores.2009.11.021.

Maeno, F., Nagai, M., Nakada, S., Burden, R., Engwell, S., Suzuki, Y., Kaneko, T., (2014) Constraining tephra dispersion and deposition from three subplinian explosions in 2011 at Shinmoedake volcano, Kyushu, Japan. Bull. Volcanol. 76 (6), 823. http://dx.doi.org/10.1007/s00445-014-0823-9.

Maeno, F., Nakada, S., Yoshimoto, M., Shimano, T., Hokanishi, N., Zaennudin, A., & Iguchi, M. (2019). A sequence of a plinian eruption preceded by dome destruction at Kelud volcano, Indonesia, on February 13, 2014, revealed from tephra fallout and pyroclastic density current deposits. Journal of Volcanology and Geothermal Research, 382, 24-41. https://doi.org/10.1016/j.jvolgeores.2017.03.002

Mastin, L. G., Guffanti, M., Servranckx, R., Webley, P., Barsotti, S., Dean, K., ... & Schneider, D. (2009). A multidisciplinary effort to assign realistic source parameters to models of volcanic ash-cloud transport and dispersion during eruptions. Journal of Volcanology and Geothermal Research, 186(1-2), 10-21.

Mastin, L. G. (2014). Testing the accuracy of a 1-D volcanic plume model in estimating mass eruption rate. Journal of Geophysical Research: Atmospheres, 119(5), 2474-2495.

Mastin, L., Pavolonis, M., Engwell, S. et al. (2022) Progress in protecting air travel from volcanic ash clouds. Bull Volcanol 84, 9 . https://doi.org/10.1007/s00445-021-01511-x

Mereu, L., Scollo, S.,. Bonadonna, C.,. Donnadieu, F., . Freret-Lorgeril, V. and Marzano, F. S. (2022) "Ground-Based Remote Sensing and Uncertainty Analysis of the Mass Eruption Rate Associated With the 3–5 December 2015 Paroxysms of Mt. Etna," in IEEE Journal of Selected Topics in Applied Earth Observations and Remote Sensing, vol. 15, pp. 504-518, , doi: 10.1109/JSTARS.2021.3133946.

Morton, B. R., Taylor, G.I, and Turner, J.S. (1956) Turbulent gravitational convection from maintained and instantaneous sources. Proceedings of the Royal Society of London. Series A. Mathematical and Physical Sciences 234.1196 : 1-23.

Naranjo, J., Sigurdsson, H., Carey, S., Fritz, W., (1986). Eruption of the Nevado del Ruiz volcano, Colombia, on 13 November 1985: tephra fall and lahars. Science 233, 961–964. http://dx.doi.org/10.1126/science.233.4767.961.

Newhall, C. G., & Self, S. (1982). The volcanic explosivity index (VEI) an estimate of explosive magnitude for historical volcanism. Journal of Geophysical Research: Oceans, 87(C2), 1231-1238.

Pioli, L., & Harris, A. J. (2019). Real-time geophysical monitoring of particle size distribution during volcanic explosions at Stromboli volcano (Italy). Frontiers in Earth Science, 7, 52.

Poulidis, A. P., Takemi, T., & Iguchi, M. (2019). The effect of wind and atmospheric stability on the morphology of volcanic plumes from vulcanian eruptions. Journal of Geophysical Research: Solid Earth, 124, 8013– 8029. https://doi.org/10.1029/2018JB016958

Robertson, R. E. A., Cole, P., Sparks, R. S. J., Harford, C., Lejeune, A. M., McGuire, W. J., ... & Young, S. R. (1998). The explosive eruption of soufriere hills volcano, montserrat, west indies, 17 september, 1996. Geophysical Research Letters, 25(18), 3429-3432.

Romero, J. E., Vera, F., Polacci, M., Morgavi, D., Arzilli, F., Alam, M. A., ... & Keller, W. (2018). Tephra from the 3 March 2015 sustained column related to explosive lava fountain activity at Volcán Villarrica (Chile). Frontiers in Earth Science, 6, 98.

Rosi, M., M. Paladio-Melosantos, A. Di Muro, R. Leoni, and T. Bacolcol (2001), Fall vs flow activity during the 1991 climactic eruption of Pinatubo Volcano (Philippines), Bull. Volcanol., 62, 549–566, doi:10.1007/s004450000118.

Rossi, E., Bonadonna, C., Degruyter, W. (2019) A new strategy for the estimation of plume height from clast dispersal in various atmospheric and eruptive conditions, Earth Planet. Sci. Lett., 505 , pp. 1-12

Scollo, S.; Prestifilippo, M.; Bonadonna, C.; Cioni, R.; Corradini, S.; Degruyter, W.; Rossi, E.; Silvestri, M.; Biale, E.; Carparelli, G.; Cassisi, C.; Merucci, L.; Musacchio, M.; Pecora, E.

(2019) Near-Real-Time Tephra Fallout Assessment at Mt. Etna, Italy. Remote Sens. , 11, 2987. https://doi.org/10.3390/rs11242987

Self, S., Rampino, M., (2012). The 1963-1964 eruption of Agung volcano (Bali, Indonesia). Bull. Volcanol. 74 (6), 1521–1536. http://dx.doi.org/10.1007/s00445-012-0615-z.

Sparks, R. S. J. (1986) The dimensions and dynamics of volcanic eruption columns. Bulletin of Volcanology 48.1 : 3-15.

Trancoso, R., Behr, Y., Hurst, T. et al. Towards real-time probabilistic ash deposition forecasting for New Zealand. J Appl. Volcanol. 11, 13 (2022). https://doi.org/10.1186/s13617-022-00123-0

Tupper, A., & Wunderman, R. (2009). Reducing discrepancies in ground and satellite-observed eruption heights. Journal of Volcanology and Geothermal Research, 186(1-2), 22-31.

Tupper, A., Textor, C., Herzog, M., Graf, H.-F., & Richards, M. S. (2009). Tall clouds from small eruptions: the sensitivity of eruption height and fine ash content to tropospheric instability. Natural Hazards, 51(2), 375–401. https://doi.org/10.1007/s11069-009-9433-9

Wilson, L., Sparks, R. S. J., Huang, T. C., & Watkins, N. D. (1978). The control of volcanic column heights by eruption energetics and dynamics. Journal of Geophysical Research: Solid Earth, 83(B4), 1829-1836.

Woodhouse, M. J., Hogg, A. J., Phillips, J. C., & Sparks, R. S. J. (2013). Interaction between volcanic plumes and wind during the 2010 Eyjafjallajökull eruption, Iceland. Journal of Geophysical Research: Solid Earth, 118(1), 92-109.

Woods, A.W. (1988) The fluid dynamics and thermodynamics of eruption columns. Bull Volcanol 50, 169–193 . https://doi.org/10.1007/BF01079681

Woods, A. W., & Bursik, M. I. (1991). Particle fallout, thermal disequilibrium and volcanic plumes. Bulletin of Volcanology, 53(7), 559-570.

Woods, A. W. (1993), Moist convection and the injection of volcanic ash into the atmosphere, J. Geophys. Res., 98(B10), 17627– 17636, doi:10.1029/93JB00718.

Woods, A.W., Bower, S.M., 1995. The decompression of volcanic jets in a crater during explosive volcanic eruptions. Earth Planet. Sci. Lett. 131 (3), 189–205. http://dx. doi.org/10.1016/0012-821X(95)00012-2.